catalysts

MDPI

Article

Modified Cellulose with BINAP-Supported Rh as an Efficient Heterogeneous Catalyst for Asymmetric Hydrogenation

Cuiping Yu [1], Weilong Wu [2], Min Gao [1,*] and Yu Liu [1,*]

[1] State Key Laboratory of Biobased Material and Green Papermaking, Qilu University of Technology, Shandong Academy of Sciences, Jinan 250353, China; P18363008761@163.com
[2] College of Chemistry and Chemical Engineering, Luoyang Normal University, Luoyang 471934, China; weilong20101001@163.com
* Correspondence: shdgaomin@whu.edu.cn (M.G.); leoliuyu@163.com (Y.L.)

Abstract: Asymmetric catalysis is the preferred method for the synthesis of pure chiral molecules in the fine chemical industry. Cellulose has long been sought as a support in enantioselective catalysis. Dialdehyde cellulose (DAC) is produced by the selective oxidation of cellulose and is used to bind 5,5′-diamino Binap by forming a Schiff base. Here, we report the synthesis of modified cellulose-supported Rh as a novel biomass-supported catalyst and the characterization of its morphology, composition, and thermal stability. DAC-BINAP-Rh was a very effective catalyst in the asymmetric hydrogenation of enamides and could be easily recycled. This work provides a novel supported catalyst that broadens the applications of cellulose in asymmetric catalysis.

Keywords: asymmetric hydrogenation; cellulose; BINAP; heterogeneous catalysis

Citation: Yu, C.; Wu, W.; Gao, M.; Liu, Y. Modified Cellulose with BINAP-Supported Rh as an Efficient Heterogeneous Catalyst for Asymmetric Hydrogenation. *Catalysts* **2022**, *12*, 83. https://doi.org/10.3390/catal12010083

Received: 3 December 2021
Accepted: 7 January 2022
Published: 12 January 2022

1. Introduction

Chirality plays a major role in chemistry. Asymmetric hydrogenation is an important way to prepare enantiomerically pure pharmaceuticals and other fine chemicals. So far, various chiral catalysts have been developed, many of which are very effective for the asymmetric hydrogenation of C=C, C=O, and other bonds [1–4]. Compared to the significant development of homogeneous asymmetric catalysts, heterogeneous asymmetric catalysts have developed more slowly and received less attention [5,6]. Although homogeneous catalysts have good reactivity and a high turnover number (TON), the loss of precious metals and chiral ligands limit their industrial applications [7,8]. The advantages of heterogeneous catalysts, such as their ease of separation and reusability, can reduce the amounts of scarce resources that are required; thus, considerable efforts have been devoted to finding strategies to develop heterogeneous asymmetric catalysts [9,10]. Recent trends have seen immobilization emerge as an efficient tool for the easy separation of catalysts from substrates and products, which reduces environmental contamination [11–15]. Because of this, heterogeneous catalysts have been developed in the industry. Over the past decades, many metallic species have been supported on inorganic materials and synthetic polymers, such as silica [16,17], zeolites [18,19], metal oxides [20,21], charcoal [22,23], and magnetic materials [24,25], which have been successfully used in catalytic applications. Although these catalyst systems have achieved high yields and enantioselectivity, these copolymers are predominantly derived from petroleum, an unsustainable resource.

In recent years, the transition from petrochemical-based raw materials to biomass-based materials has promoted the cleaner and sustainable development of the chemical industry [26,27]. Natural polymers receive high attention because of their abundance and biodiversity can produce various properties at low cost. In addition, they are biocompatible, biodegradable, non-toxic and highly reactive. For ecological reasons, natural polymers are generally more popular than synthetic polymers and can effectively utilize renewable

biomass [28–30]. Polysaccharides are important biomass biopolymers with many advantages, such as a high adsorption capacity, metal anion stability, many stereocenters, good chemical stability, and biodegradability, which make them an attractive support [31–34].

Celluloses are the most abundant macromolecules in the plant kingdom. We focused on the use of cellulose as a support for asymmetric catalysis because this material has several advantages, including a high stability and insolubility in common solvents and also because it contains many hydroxyl groups, which can stabilize metal particles [35,36]. Cellulose and its derivatives (polysaccharides) have also been applied in asymmetric catalysis. An early example of the immobilization of Pd-complex catalysts using cellulose as a support for asymmetric hydrogenation was reported in 1956, and the seminal work was included in Nature [37]; however, research in this area stagnated in the following decades. At the end of the century, due to increasingly prominent energy and environmental issues, the use of biomass as a carrier for catalysts has attracted great attention around the world.

BINAP [2,2′-bis(diphenylphosphino)-1,1′-binaphthyl] is an excellent homogeneous catalyst for various asymmetric hydrogenation reactions and is frequently used to explore new methods for the development of heterogeneous asymmetric catalysis [38–43]. With these considerations in mind, the purpose of this research is to develop an environmentally friendly BINAP-modified DAC supported Rh complex to achieve green catalysis (Scheme 1). Then, the catalytic activity of this synthetic compound (DAC-BINAP-Rh) was studied in the asymmetric catalytic hydrogenation of enamides. This work will provide a novel method for the utilization of other promising biopolymers as advanced supports in asymmetric hydrogenation reactions.

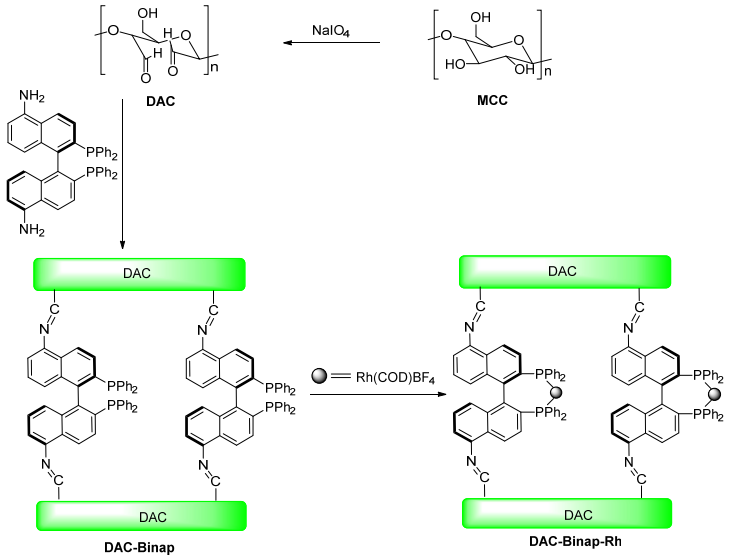

Scheme 1. Preparation of DAC-BINAP-Rh.

2. Results

2.1. Characterization

This report focuses on the preparation of dialdehyde cellulose and its functionalized modified catalysts for asymmetric catalytic hydrogenation. Evidence of DAC and DAC-BINAP preparation was provided by FT-IR spectra (Figure 1). The oxidation of microcrystalline cellulose resulted in very few changes to its functional groups because the typical absorption peaks associated with cellulose were unchanged. For example, the strong broadband band at 3350 cm^{-1} and the strong absorption peak at 1635 cm^{-1} were respectively assigned to the tensile vibration of -OH and the stretching vibration of H-O-H [44]. The characteristic peak at 2903 cm^{-1} was generated by symmetric and asymmetric C-H vibrations [45]. In the FT-IR spectra of DAC, the characteristic bands at 1732 cm^{-1} and 889 cm^{-1} belong to the hydrated forms of aldehyde carbonyls, hemiacetals, and aldehydes, respectively. The FT-IR peak of DAC-BINAP at 1663 cm^{-1} belongs to N=C

bending. The disappearance of the band at 1732 cm^{-1} (in DAC) was due to the strong C=N bond formed by the Schiff base reaction between BINAP-NH_2 and –CHO. The weakened band at 3375 cm^{-1} in the DAC-BINAP spectrum was mainly caused by the reduction of -OH groups [46]. After the catalytic reaction is completed, the FT-IR spectrum shows that there is still a C=N bond absorption peak at 1663 cm^{-1}, indicating that the catalyst only acts on the reaction substrate and has no effect on the structure of the catalyst.

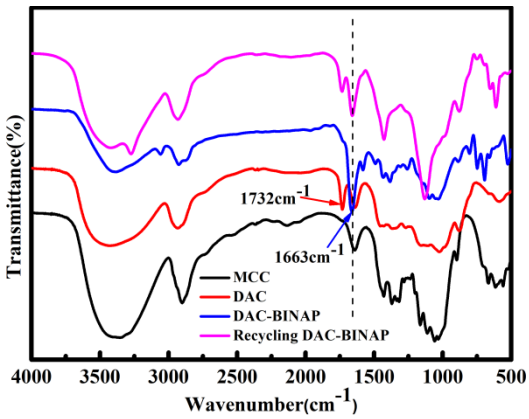

Figure 1. FT-IR spectra of MCC, DAC, DAC-BINAP and Recycling DAC-BINAP.

The phase composition and crystallinity of MCC, DAC, and DAC-BINAP were characterized by XRD, and the results are shown in Figure 2. In the XRD patterns of MCC, the two crystallization peaks at 2θ = 22.4° and 15.5° corresponded to the typical diffraction peaks of cellulose I and cellulose II, respectively. During the oxidation of microcrystalline cellulose, the structure of cellulose was destroyed due to the addition of a large amount of $NaIO_4$. The characteristic diffraction peak of the cellulose was not retained, and only a broad peak existed around 2θ = 20°. The crystalline peaks at 2θ = 34.5 were weakened or even disappeared in the case of DAC. The reduced crystallinity after oxidation is one of the characteristics of cellulose periodate oxidation. The reason is that the structure and functional groups of cellulose changed, and the packing order of cellulose chains was disrupted after the opening of the glucose pyran ring after oxidation [47,48]. The crystallization peak of DAC-HN-BINAP is similar to that of DAC, which indicates that the crystal structure of DAC was not changed during the functionalization of DAC, which is also supported by the FT-IR spectrum in Figure 1 [49].

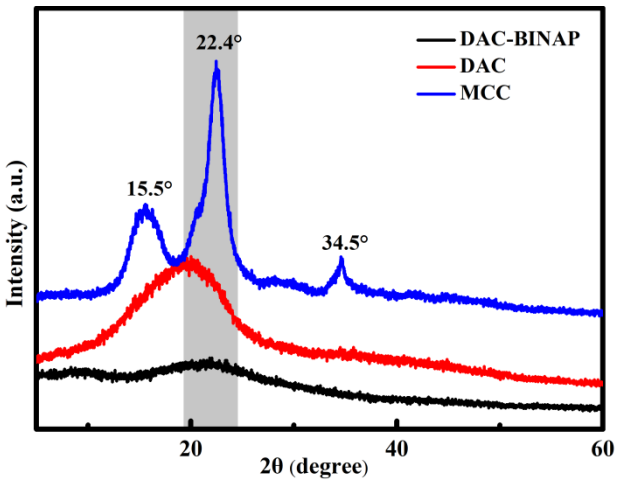

Figure 2. XRD spectra of MCC, DAC and DAC-BINAP.

Catalytic hydrogenation generally needs to be carried out with heating, so the thermal stability of the catalyst is crucial to its activity and reusability; therefore, the thermal stability

of the chiral ligand was tested by TGA, and the results are shown in Figure 3. The thermal stability curves of DAC-BINAP and DAC have similar trends, indicating that the thermal stability of DAC was not damaged during the preparation of bio-based chiral ligands. Both began to decompose rapidly near 180 °C. In addition, the mass of the bio-based chiral ligand in the final residue was about 20% higher than that of the unmodified DAC, due to the binding of *R*-5,5′-diamino BINAP; therefore, the designed bio-based chiral ligand shows good thermal stability and can be used stably at the temperature required by the experiment.

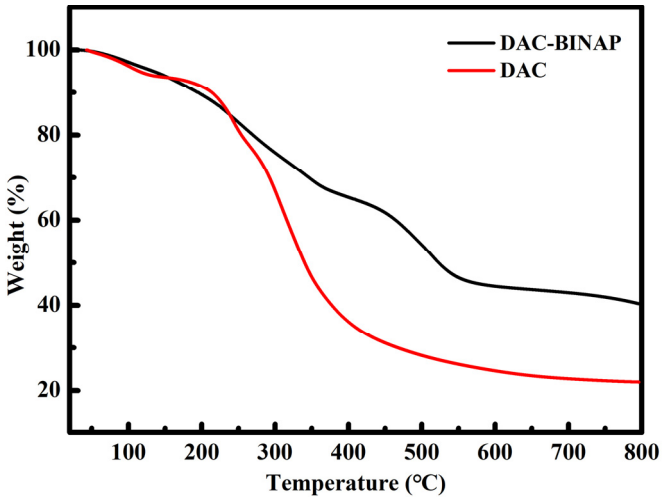

Figure 3. Thermogravimetric curves of DAC and DAC-BINAP.

Rh(I) complexes are known to catalyze the hydrogenation of various unsaturated hydrocarbons, including alkynes [50]. XPS analysis is an effective tool for verifying the elemental composition of compounds. The characteristic peaks of C 1s, O 1s, N 1s, Rh 3d, and P 2p elements can be clearly seen in the XPS spectra in Figure 4a, which proves that $Rh(COD)_2BF_4$ was successfully complexed with DAC-BINAP. The oxygen-containing functional group on the surface of DAC acts as an anchor point to fix Rh via electrostatic interactions, so that $Rh(COD)_2BF_4$ was distributed on the surface of DAC-BINAP [51]. The binding energy peaks of Rh $3d_{5/2}$ and Rh $3d_{3/2}$ for Rh/DAC-BINAP were observed at 307.79 eV and 312.47 eV, respectively, as shown in Figure 4b, indicating the presence of Rh^0 [52].

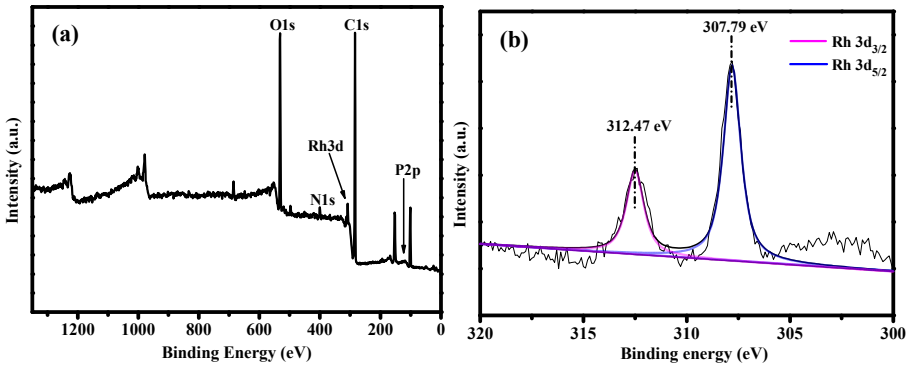

Figure 4. XPS spectra of DAC-BINAP (**a**) and Rh 3d (**b**).

The SEM image (Figure 5) shows the overall morphology of MCC after oxidation and that further grafting did not change it significantly. It can be seen from images (Figure 5a,d) that the surface of MCC was rough. The surface of DAC was smoother, and the specific surface area increased, which may be caused by the hydrolysis of hemicelluloses, which formed the cellulose skeleton, after the oxidation of $NaIO_4$. After functionalization of DAC to 5,5′-diamino BINAP, the surface of DAC-BINAP became rough again. The presence of

Rh and P elements can be clearly seen from the EDS images, which further proves that BINAP is grafted and Rh is successfully complexed.

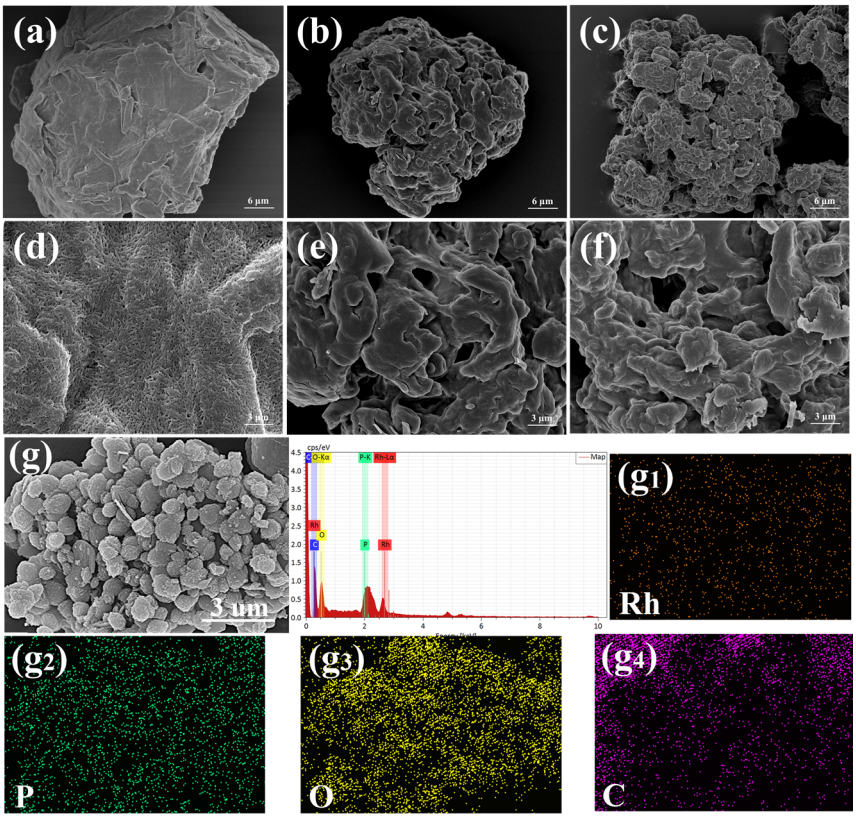

Figure 5. SEM images of MCC (**a**,**d**) DAC (**b**,**e**) DAC-BINAP (**c**,**f**) Rh/DAC-BINAP (**g**) and EDS images of different elements (**g**$_1$–**g**$_4$).

The morphology of Rh/DAC-BINAP was analyzed by transmission electron microscopy (TEM), which showed that rhodium particles were uniformly distributed on the surface of DAC-BINAP (Figure 6a). The dark points with an average particle size of 20.71 nm correspond to Rh complexation in DAC-BINAP (Figure 6b) The lattice stripe lines of metal rhodium can be clearly observed in the magnified TEM images. Its surface spacing was measured to be about 0.39 nm, which is in accordance with the theoretical value of the lattice plane of metal rhodium (Figure 6c) [53]. After repeatedly using the catalyst six times for hydrogenation, the rhodium nanoparticles agglomerated slightly and formed small clusters with uneven sizes (Figure 6d), resulting in a slight decrease in the catalytic activity.

2.2. Catalytic Activity of DAC-BINAP-Rh

In the presence of the DAC-BINAP-Rh catalyst, we selected 2-acetamino-3-phenylacrylate as the classical substrate and studied its application for asymmetric hydrogenation. We investigated the solvent effect and found that different solvents had a great influence on the conversions and enantioselectivity (ee) values. Alcoholic solvents gave lower ee, albeit with promising conversions (Table 1, Entries 3–4,6). Toluene gave high ee but poor conversions (Table 1, Entry 7). When the reaction time was increased to 12 h (Table 1, Entry 10), the catalysts exhibited excellent activity (65% conversion, 73% ee). Economical feasibility should be considered from the following points: (1) Reaction should provide higher conversion and selectivity at lesser reaction time; (2) Long reactions promote impurity formation and reduce the selectivity of desired products. Thus, 12 h was the optimal time to achieve better conversion and enantioselectivity.

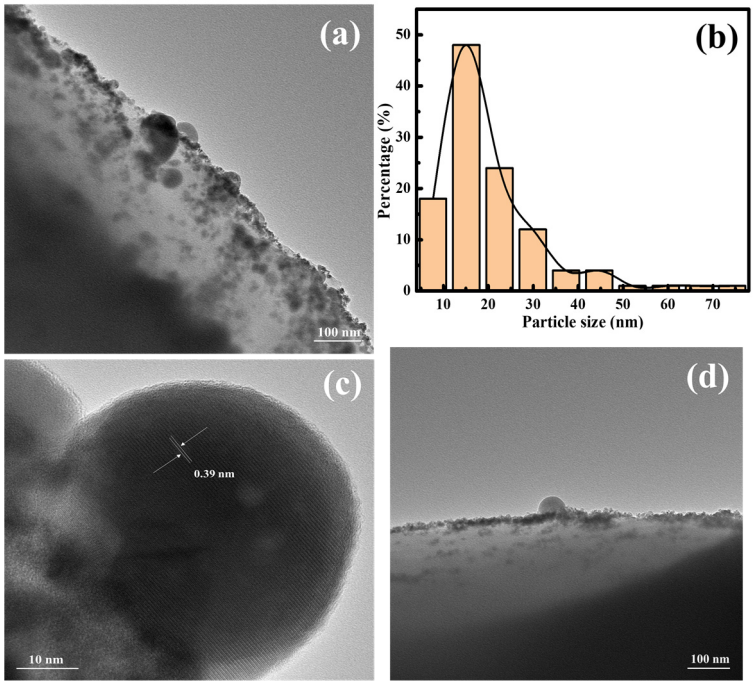

Figure 6. TEM images: (**a**) Fresh Rh/DAC-BINAP; (**b**) Particle size distribution of Rh nanoparticles (**c**) Lattice fringe of Rh nanoparticles; (**d**) the reused Rh/DAC-BINAP come from hydrogenation six times.

Table 1. Solvent Screening for Rh-Catalyzed Asymmetric Hydrogenation of 2-acetamido-3-phenylprop-2-enoate [a].

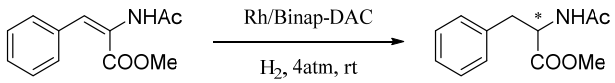

Entry	Solvent	Time (h)	Con (%) [b]	ee (%) [c]
1	THF	4	23	3
2	CH_2Cl_2	4	56	76
3	MeOH	4	>99	10
4	EtOH	4	>99	10
5	CH_3CN	4	54	28
6	*i*PrOH	4	>99	28
7	toluene	4	45	80
8	dioxane	4	37	44
9	xylene	4	48	44
10 [c]	toluene	12	65	73

[a] Unless otherwise mentioned, all reactions were carried out at room temperature under hydrogen (4 atm) for 4 h. [b] Determined by ^{1}H NMR spectroscopy. [c] Determined by HPLC analysis using a chiral stationary phase. Explain: * represents the chiral center.

Catalytic materials are easily separated from the substrate/product solution. The recovery process can be repeated five times without significantly reducing selectivity and activity (Table 2).

Table 2. Heterogeneous catalyst recovery [b].

Cycle	1	2	3	4	5	6
Con (%) [(a)]	45	45	45	45	45	40
ee (%) [(a)]	80	78	78	76	75	75

[(a)] Determined by HPLC analysis using a chiral stationary phase. [b] Unless otherwise mentioned, the conditions used for cyclic reactions are the same as in Table 1, Entry 7.

3. Materials and Methods

3.1. Materials

Microcrystalline cellulose (MCC, degree of polymerization = 180) was purchased from Shandong Liao cheng A Hua Pharmaceutical Co., Ltd. $Rh(COD)_2BF_4$ was purchased from Sigma-Aldrich. All reagents were ultra-dry solvents purchased directly from Aladdin. All reagents were used as received. NMR spectra were recorded on Bruker ADVANCE III (400 MHz) spectrometers for ^1H NMR and ^{13}C NMR. $CDCl_3$ was the solvent used for NMR analysis, with tetramethyl silane as the internal standard. Chemical shifts were reported upfield to TMS (0.00 ppm) for ^1H NMR and relative to $CDCl^3$ (77.0 ppm) for ^{13}C NMR. Optical rotation was determined using a Perkin Elmer 343 polarimeter. HPLC analysis was conducted on an Agilent 1260 Series instrument. Column chromatography was performed with silica gel Merck 60 (300–400 mesh). All new products were further characterized by HRMS.

3.2. Experimental

3.2.1. Preparation of Dialdehyde Cellulose (DAC)

As reported in the literature [54], the preparation method of dialdehyde cellulose is as follows: Firstly, 400 mL of deionized water was added into a 500-mL brown three-mouth flask, and 5 g microcrystalline cellulose, 7.2 g LiCl, 7.2 g sodium periodate ($NaIO_4$) were weighed in deionized water, then the suspension was magnetically stirred in an oil bath at 75 °C. The mouth of the flask was covered with aluminum foil to prevent the photocatalytic decomposition of $NaIO_4$. After three hours, the reaction system was repeatedly pumped and washed with deionized water and anhydrous ethanol (1:9) to remove excess iodine compounds. The above product was vacuum-dried at 60 °C to obtain DAC. The aldehyde group content of oxidized cellulose was determined to be 8.4 mmol/g by quantitatively reacting hydroxylamine hydrochloride-methanol solution with the aldehyde group.

3.2.2. Preparation of R-5,5′-Diamino BINAP

(R)-5,5′-Diamino-BINAP was synthesized according to the literature [55].

3.2.3. Preparation of DAC-BINAP Catalyst

As reported in the literature [55], 0.012 g DAC was soaked in a pressure flask containing 10 mL of *N*,*N*-dimethylformamide (DMF), protected by nitrogen and stirred magnetically in an oil bath at 50 °C. Then, ammonium persulfate (0.01 g) and triethylenetetramine (TETA) (0.01 g) were added and allowed to dissolve in DMF. After 8 min, BINAP-NH_2 dissolved in DMF and was added and stirred for another 3 h. The final products were successively washed with deionized water and ethyl acetate and vacuum dried to obtain DAC-BINAP. A stock solution was made by mixing $[Rh(COD)_2]BF_4$ with DAC-BINAP in a 1:1.1 molar ratio in CH_2Cl_2 at room temperature for 30 min in a nitrogen-filled glovebox. The resulting solid was filtered and washed with ample EtOAc. The product was kept in an argon-protected glove box without drying.

3.2.4. General Procedure of DAC-BINAP-Rh Catalyst for Hydrogenation of Enamides

The catalyst solid (0.001 mmol) was transferred into vials charged with the same substrates (0.1 mmol each) in different anhydrous solvents (1.0 mL). The vials were subsequently transferred into an autoclave into which hydrogen gas was charged. The reaction

was then stirred under H_2 (4 atm) at room temperature for 4 h. The hydrogen gas was released slowly and carefully. The reaction system was separated by filtration (eluant: EtOAc) to obtain each respective catalyst and product. The enantiomeric excess (ee) values of compounds were determined by HPLC analysis on a chiral stationary phase.

3.2.5. Separation of the Catalyst and Recycling Tests

Isolation and reuse of the catalyst are crucial requirements for practical applications. In this work, the reaction solution was filtered in a N_2 atmosphere, and the supported catalyst was filtered off and washed successively with EtOH and CH_2Cl_2. Then, the filter cake was dried and reused directly without further purification.

4. Conclusions

In conclusion, we developed a simple and environmentally-friendly BINAP-modified cellulose support for Rh complexation. We have proved that the catalyst can chemically react with enamide without adversely affecting the support. Several analytical techniques have been used to analyze these immobilized compounds, and finally proved that we have indeed successfully covalently immobilized the BINAP-Rh complex on the modified cellulose. It was an efficient catalyst for the hydrogenation of methyl 2-acetylamino-3-phenylacrylate, which exhibited a high stereoselectivity (ee 80%). The catalytic results show that the reduction in activity is decisive compared with the homogeneous system. However, compared with other heterogeneous catalysts, the conversion and enantioselectivity levels are equally good even if they are not improved. In addition, the catalyst showed repeated high selectivity levels in six cycles. More importantly, this research has explored the application of bio-based materials for asymmetric catalytic hydrogenation and has provided a new green heterogeneous catalyst carrier. These advantages make this catalyst highly valuable for practical applications.

Supplementary Materials: Detailed and complete characterization of compounds and hydrogenated products (NMR spectra, HPLC chromatograms of racemic and enantiomerically enriched compounds). This material is freely available via the Internet at https://www.mdpi.com/article/10.3390/catal12010083/s1.

Author Contributions: Conceptualization, C.Y. and M.G.; methodology, C.Y.; software, W.W.; validation, C.Y., M.G. and Y.L.; formal analysis, C.Y.; investigation, M.G.; resources, W.W.; data curation, Y.L.; writing—original draft preparation, C.Y.; writing—review and editing, M.G.; visualization, W.W.; supervision, Y.L.; project administration, Y.L.; funding acquisition, Y.L. All authors have read and agreed to the published version of the manuscript.

Funding: The authors are extremely grateful for financial support from the Key Scientific Research Project of Higher Education of Henan Province, grant number19A150004, and the Foundation (ZZ20210113) of State Key Laboratory of Biobased Material and Green Papermaking, Qilu University of Technology, Shandong Academy of Sciences.

Data Availability Statement: Data are contained within the article or Supplementary Materials.

Acknowledgments: The funders had no role in the design of the study; in the collection, analyses, or interpretation of data; in the writing of the manuscript; or in the decision to publish the results.

Conflicts of Interest: The authors declare no conflict of interest.

References

1. Wang, D.S.; Chen, Q.A.; Lu, S.M. Asymmetric hydrogenation of heteroarenes and arenes. *Chem. Rev.* **2012**, *112*, 2557–2590. [CrossRef]
2. Hu, Y.; Chen, J.; Li, B. Nickel-Catalyzed Asymmetric Hydrogenation of 2-Amidoacrylates. *Angew. Chem. Int. Ed.* **2020**, *132*, 5409–5413. [CrossRef]
3. Abdine, R.A.A.; Hedouin, G.; Colobert, F. Metal-Catalyzed Asymmetric Hydrogenation of C=N Bonds. *ACS Catal.* **2020**, *11*, 215–247. [CrossRef]

4. Mi, R.; Chen, C.; Keplinger, T.; Pei, Y.; He, S. Scalable aesthetic transparent wood for energy efficient buildings. *Nat. Commun.* **2020**, *11*, 3836. [CrossRef]
5. Seo, C.S.; Morris, R.H. Catalytic homogeneous asymmetric hydrogenation: Successes and opportunities. *Organometallics* **2018**, *38*, 47–65. [CrossRef]
6. Rochat, R.; Lopez, M.J.; Tsurugi, H.; Mashima, K. Recent developments in homogeneous organomagnesium catalysis. *ChemCatChem* **2016**, *8*, 10–20. [CrossRef]
7. Erick, M.C.; Hisashi, Y. Industrial Applications of Asymmetric Synthesis. In *Comprehensive Chirality*; Elsevier Ltd.: Amsterdam, The Netherlands, 2012; Volume 9, pp. 73–82.
8. Tan, J.; Yasuda, N. Contemporary Asymmetric Phase Transfer Catalysis: Large-Scale Industrial Applications. *Org. Process. Res. Dev.* **2015**, *19*, 1731–1746. [CrossRef]
9. Meemken, F.; Baiker, A. Recent Progress in Heterogeneous Asymmetric Hydrogenation of C=O and C=C Bonds on Supported Noble Metal Catalysts. *Chem. Rev.* **2017**, *117*, 11522–11569. [CrossRef]
10. Szőllősi, G. Asymmetric one-pot reactions using heterogeneous chemical catalysis: Recent steps towards sustainable processes. *Catal. Sci. Technol.* **2018**, *8*, 389–422. [CrossRef]
11. Hu, A.; Liu, S.; Lin, W. Immobilization of chiral catalysts on magnetite nanoparticles for highly enantioselective asymmetric hydrogenation of aromatic ketones. *RSC Adv.* **2012**, *2*, 2576–2580. [CrossRef]
12. Ahn, S.H.; Choi, M.S.; Im, J.S.; Sheikh, R. Improved method for immobilization of a chiral complex on PTA/alumina for asymmetric hydrogenation of a β-ketoester. *J. Mol. Catal. A Chem.* **2013**, *373*, 55–60. [CrossRef]
13. Kirby, F.; Moreno-Marrodan, C.; Baán, Z.; Bleeker, B.F.; Barbaro, P.; Berben, P.H.; Witte, P.T. NanoSelect Precious Metal Catalysts and their Use in Asymmetric Heterogeneous Catalysis. *J. ChemCatChem* **2014**, *6*, 2904–2909. [CrossRef]
14. Yoon, M.; Srirambalaji, R.; Kim, K. Homochiral metal–organic frameworks for asymmetric heterogeneous catalysis. *Chem. Rev.* **2012**, *112*, 1196–1231. [CrossRef]
15. Clarke, A.K.; James, M.J.; O'Brien, P. Silica-Supported Silver Nitrate as a Highly Active Dearomatizing Spirocyclization Catalyst: Synergistic Alkyne Activation by Silver Nanoparticles and Silica. *Angew. Chem.* **2016**, *128*, 14002–14006. [CrossRef]
16. Cecilia, J.A.; Jiménez-Morales, I. Influence of the silica support on the activity of Ni and Ni2P based catalysts in the hydrodechlorination of chlorobenzene. Study of factors governing catalyst deactivation. *J. Mol. Catal. A-Chem.* **2013**, *368*, 78–87. [CrossRef]
17. Blakeman, P.G.; Burkholder, E.M. The role of pore size on the thermal stability of zeolite supported Cu SCR catalysts. *Catal. Today* **2014**, *231*, 56–63. [CrossRef]
18. Zhang, J.; Wang, L. A Pd@ zeolite catalyst for nitroarene hydrogenation with high product selectivity by sterically controlled adsorption in the zeolite micropores. *Angew. Chem.* **2017**, *129*, 9879–9883. [CrossRef]
19. Védrine, J.C. Heterogeneous catalysis on metal oxides. *Catalysts* **2017**, *7*, 341. [CrossRef]
20. Muroyama, H.; Tsuda, Y. Carbon dioxide methanation over Ni catalysts supported on various metal oxides. *J. Catal.* **2016**, *343*, 178–184. [CrossRef]
21. Liao, Y.; Jia, L. Charcoal-supported catalyst with enhanced thermal-stability for the catalytic combustion of volatile organic compounds. *Appl. Catal. A-Gen.* **2016**, *522*, 32–39. [CrossRef]
22. Lee, J.H.; Lee, I.G.; Jeon, W. Catalytic upgrading of bio-tar over a MgNiMo/activated charcoal catalyst under supercritical ethanol conditions. *Catal. Today* **2018**, *316*, 237–243. [CrossRef]
23. Sydnes, M.O. The Use of palladium on magnetic support as catalyst for Suzuki–Miyaura cross-coupling reactions. *Catalysts* **2017**, *7*, 35. [CrossRef]
24. Du, Y.; Ma, W. Magnetic CoFe2O4 nanoparticles supported on titanate nanotubes (CoFe2O4/TNTs) as a novel heterogeneous catalyst for peroxymonosulfate activation and degradation of organic pollutants. *J. Hazard. Mater.* **2016**, *308*, 58–66. [CrossRef]
25. Deeba, F.; Kumar, B.; Arora, N.; Singh, S.; Kumar, A.; Han, S.S.; Negi, Y.S. Novel bio-based solid acid catalyst derived from waste yeast residue for biodiesel production. *Renew. Energy* **2020**, *159*, 127–139. [CrossRef]
26. Liuzzi, S.; Rubino, C.; Martellotta, F.; Stefanizzi, P.; Casavola, C.; Pappalettera, G. Characterization of biomass-based materials for building applications: The case of straw and olive tree waste. *Ind. Crop. Prod.* **2020**, *147*, 112229. [CrossRef]
27. Zhao, X.; Zhou, H.; Fan, L.S. Biomass-based chemical looping technologies: The good, the bad and the future. *Energy Environ. Sci.* **2017**, *10*, 1885–1910. [CrossRef]
28. Liu, F.; Chen, Q.; Liu, C.; Wang, X. Natural polymers for organ 3D bioprinting. *Polymers* **2018**, *10*, 1278. [CrossRef]
29. Teodorescu, M.; Bercea, M.; Morariu, S. Biomaterials of Poly (vinyl alcohol) and Natural Polymers. *Polym. Rev.* **2018**, *58*, 247–287. [CrossRef]
30. Hammouda, S.B.; Fourcade, F. Effective heterogeneous electro-Fenton process for the degradation of a malodorous compound, indole, using iron loaded alginate beads as a reusable catalyst. *Appl. Catal. B Environ.* **2016**, *182*, 47–58. [CrossRef]
31. Pourjavadi, A.; Motamedi, A. Magnetic starch nanocomposite as a green heterogeneous support for immobilization of large amounts of copper ions: Heterogeneous catalyst for click synthesis of 1, 2, 3-triazoles. *RSC Adv.* **2016**, *6*, 19128–19135. [CrossRef]
32. Verma, M.L.; Kumar, S.; Das, A.; Randhawa, J.S. Chitin and chitosan-based support materials for enzyme immobilization and biotechnological applications. *Environ. Chem. Lett.* **2020**, *18*, 315–323. [CrossRef]
33. Capeling, M.M.; Czerwinski, M.; Huang, S. Nonadhesive alginate hydrogels support growth of pluripotent stem cell-derived intestinal organoids. *Stem Cell Rep.* **2019**, *12*, 381–394. [CrossRef] [PubMed]

34. Kim, U.J.; Lee, Y.R.; Kang, T.H.; Wada, M. Protein adsorption of dialdehyde cellulose-crosslinked chitosan with high amino group contents. *Carbohyd. Polym.* **2017**, *163*, 34–42. [CrossRef]
35. Keshk, S.M.; Bondock, S.; El-Zahhar, A.A.; Haija, M.A. Synthesis and characterization of novel Schiff's bases derived from dialdehyde cellulose-6-phosphate. *Cellulose* **2019**, *26*, 3703–3712. [CrossRef]
36. Akabori, S.; Sakurai, S.; Izumi, Y. An asymmetric catalyst. *Nature* **1956**, *178*, 323–324. [CrossRef]
37. Xu, Z.; Yu, X.; Sang, X.; Wang, D. BINAP-copper supported by hydrotalcite as an efficient catalyst for the borrowing hydrogen reaction and dehydrogenation cyclization under water or solvent-free conditions. *Green Chem.* **2018**, *20*, 2571–2577. [CrossRef]
38. Wang, X.; Lu, S.M.; Li, J.; Liu, Y.; Li, C. Conjugated microporous polymers with chiral BINAP ligand built-in as efficient catalysts for asymmetric hydrogenation. *Catal. Sci. Technol.* **2015**, *5*, 2585–2589. [CrossRef]
39. Sun, Q.; Meng, X.; Liu, X.; Zhang, X. Mesoporous cross-linked polymer copolymerized with chiral BINAP ligand coordinated to a ruthenium species as an efficient heterogeneous catalyst for asymmetric hydrogenation. *Chem. Commun.* **2012**, *48*, 10505–10507. [CrossRef] [PubMed]
40. Hu, A.; Yee, G.T.; Lin, W. Magnetically recoverable chiral catalysts immobilized on magnetite nanoparticles for asymmetric hydrogenation of aromatic ketones. *J. Am. Chem. Soc.* **2005**, *127*, 12486–12487. [CrossRef] [PubMed]
41. Li, C.; Zhang, L.; Liu, H.; Zheng, X.; Fu, H.; Chen, H.; Li, R. Heterogeneous asymmetric hydrogenation of aromatic ketones enhanced by silanols on highly monodispersed silica spheres. *J. Catal. Commun.* **2014**, *54*, 27–30. [CrossRef]
42. McDonald, A.R.; Müller, C.; Vogt, D.; van Koten, G. BINAP-Ru and-Rh catalysts covalently immobilised on silica and their repeated application in asymmetric hydrogenation. *Green Chem.* **2008**, *10*, 424–432. [CrossRef]
43. Wen, Y.; Yuan, Z.; Qu, J. Evaluation of ultraviolet light and hydrogen peroxide enhanced ozone oxidation treatment for the production of cellulose nanofibrils. *ACS Sustain. Chem. Eng.* **2018**, *7*, 2688–2697. [CrossRef]
44. Tkachenko, T.; Sheludko, Y.; Yevdokymenko, V. Physico-chemical properties of flax microcrystalline cellulose. *Appl. Nano.* **2021**. pre publish. [CrossRef]
45. Qiao, H.; Guo, T.; Zheng, Y. A novel microporous oxidized bacterial cellulose/arginine composite and its effect on behavior of fibroblast/endothelial cell. *Carbohyd. Polym.* **2018**, *184*, 323–332. [CrossRef]
46. Zhu, L.; Liu, Y.; Jiang, Z. Highly temperature resistant cellulose nanofiber/polyvinyl alcohol hydrogel using aldehyde cellulose nanofiber as cross-linker. *Cellulose* **2019**, *26*, 5291–5303. [CrossRef]
47. Errezma, M.; Mabrouk, A.B.; Magnin, A. Surfactant-free emulsion Pickering polymerization stabilized by aldehyde-functionalized cellulose nanocrystals. *Carbohyd. Polym.* **2018**, *202*, 621–630. [CrossRef] [PubMed]
48. Ai, L.; Su, J.; Wang, M.; Jiang, J. Bamboo-structured nitrogen-doped carbon nanotube coencapsulating cobalt and molybdenum carbide nanoparticles: An efficient bifunctional electrocatalyst for overall water splitting. *ACS Sustain. Chem. Eng.* **2018**, *6*, 9912–9920. [CrossRef]
49. Petrucci, M.G.; Kakkar, A.K. Heterogenizing homogeneous catalysis using molecular self-assembly of long alkane chain phosphines bound to Rh (I) complexes. *Chem. Mater.* **1999**, *11*, 269–276. [CrossRef]
50. Seyednejhad, S.; Khalilzadeh, M.A.; Zareyee, D.; Sadeghifar, H.; Venditti, R. Cellulose nanocrystal supported palladium as a novel recyclable catalyst for Ullmann coupling reactions. *Cellulose* **2019**, *26*, 5015–5031. [CrossRef]
51. Jiang, R.; Qu, X.; Zeng, F.; Li, Q. MOF-74-immobilized ternary RhNiP nanoparticles as highly efficient hydrous hydrazine dehydrogenation catalysts in alkaline solutions. *Int. J. Hydrog. Energy* **2019**, *44*, 6383–6391. [CrossRef]
52. Niranjan, M.K. First principles study of structural, electronic and elastic properties of cubic and orthorhombic RhSi. *Intermetallics* **2012**, *26*, 150–156. [CrossRef]
53. Liimatainen, H.; Sirviö, J.; Sundman, O. Use of nanoparticular and soluble anionic celluloses in coagulation-flocculation treatment of kaolin suspension. *Water Res.* **2012**, *46*, 2159–2166. [CrossRef] [PubMed]
54. Huang, Y.Y.; Deng, G.J.; Wang, X.Y. Improved synthesis of 5,5-diamino BINAP and application to asymmetric hydrogenation. *Chin. J. Chem.* **2004**, *22*, 891–893. [CrossRef]
55. Yao, M.; Wang, Z.; Liu, Y. Preparation of dialdehyde cellulose graftead graphene oxide composite and its adsorption behavior for heavy metals from aqueous solution. *Carbohydr. Polym.* **2019**, *212*, 345–351. [CrossRef] [PubMed]